Bone Reports 18 (2023) 101647

Contents lists available at ScienceDirect

Bone Reports

journal homepage: www.elsevier.com/locate/bonr

Bone-cartilage crosstalk informed by aging mouse bone transcriptomics and human osteoarthritis genome-wide association studies

Serra Kaya [a], Karsyn N. Bailey [a,b], Charles A. Schurman [a,b], Daniel S. Evans [c], Tamara Alliston [a,b,*]

[a] Department of Orthopaedic Surgery, University of California San Francisco, CA, United States of America
[b] UC Berkeley-UCSF Graduate Program in Bioengineering, San Francisco, CA, United States of America
[c] California Pacific Medical Center Research Institute, San Francisco, CA, United States of America

ARTICLE INFO

Keywords:
Osteoarthritis
Subchondral bone
Aging
Osteocytes
Genetic research

ABSTRACT

Subchondral bone participates in crosstalk with articular cartilage to maintain joint homeostasis, and disruption of either tissue results in overall joint degeneration. Among the subchondral bone changes observed in osteoarthritis (OA), subchondral bone plate (SBP) thickening has a time-dependent relationship with cartilage degeneration and has recently been shown to be regulated by osteocytes. Here, we evaluate the effect of age on SBP thickness and cartilage degeneration in aging mice. We find that SBP thickness significantly increases by 18-months of age, corresponding temporally with increased cartilage degeneration. To identify factors in subchondral bone that may participate in bone cartilage crosstalk or OA, we leveraged mouse transcriptomic data from one joint tissue compartment – osteocyte-enriched bone – to search for enrichment with human OA in UK Biobank and Arthritis Research UK Osteoarthritis Genetics (arcOGEN) GWAS using the mouse2human (M2H, www.mouse2human.org) strategy. Genes differentially expressed in aging mouse bone are significantly enriched for human OA, showing joint site-specific (knee vs. hip) relationships, exhibit temporal associations with age, and unique gene clusters are implicated in each type of OA. Application of M2H identifies genes with known and unknown functions in osteocytes and OA development that are clinically associated with human OA. Altogether, this work prioritizes genes with a potential role in bone/cartilage crosstalk for further mechanistic study based on their association with human OA in GWAS.

1. Introduction

Osteoarthritis (OA) remains a leading cause of disability nationally, despite significant scientific investigation to identify causal mechanisms, diagnostics, and therapies for this disease (Murray et al., 2012). OA is characterized by the degeneration of both cartilage and subchondral bone (Goldring and Goldring, 2016), yet the precise mechanisms underlying crosstalk between these two tissues in joint disease are not well understood. Until recently, osteocytes have been overlooked as cellular contributors to joint disease. We recently identified a causal role for subchondral bone osteocytes in OA, revealing osteocytes as key drivers of cartilage degeneration, the response of subchondral bone to joint injury, and joint shape (Mazur et al., 2019; Bailey et al., 2021). However, the mechanisms by which osteocytes support joint health remain unknown.

Osteocytes rapidly remodel their mineralized extracellular matrix by secreting acid and proteases such as MMP13 and cathepsin K, and then later depositing new matrix (Tang et al., 2012; Dole et al., 2017; Mazur et al., 2019). This dynamic process, called perilacunar/canalicular remodeling (PLR), maintains the intricate lacunocanalicular network (LCN) containing dendrites, which enables osteocyte communication and mechanosensation (Bonewald, 2011; Tang et al., 2012; Kaya et al., 2017). Subchondral bone from OA patients undergoing joint replacement surgery shows a dramatic loss of osteocyte function, including suppression of PLR (Mazur et al., 2019). Furthermore, osteocyte dysfunction, either through targeted deletion in osteocytes of MMP13, an essential PLR enzyme, or TGFβ type II receptor (TβRII) is sufficient to drive LCN degeneration, subchondral bone thickening, changes in subchondral bone shape, and cartilage degeneration (Mazur et al., 2019; Bailey et al., 2021). Alongside OA development, aging results in lower

* Corresponding author at: University of California San Francisco, Department of Orthopaedic Surgery, 513 Parnassus Avenue, S1155, San Francisco, CA 94143, United States of America.
E-mail address: Tamara.Alliston@ucsf.edu (T. Alliston).

https://doi.org/10.1016/j.bonr.2022.101647
Received 29 August 2022; Received in revised form 28 November 2022; Accepted 11 December 2022
Available online 13 December 2022

mRNA expression levels of osteocytic TβRII and MMP13 and LCN degeneration, suggesting that defective osteocyte function may contribute to age-related OA (Schurman et al., 2021).

One possible mechanism by which osteocytes may impact cartilage health is through their control of subchondral bone plate (SBP) thickness (Burr and Gallant, 2012; Bailey et al., 2021). SBP thickness has been shown to change in response to injury and changes in load (Jia et al., 2018; Bailey et al., 2021); however, studies investigating SBP thickness in the setting of age remain inconclusive. For instance, mice with a cartilage-specific loss of EGFR have age-related SBP thickening by 12-months, yet wildtype littermates do not show differences in SBP thickness by 12-months (Jia et al., 2018). In another study of an aging mouse model, injury causes an age-dependent increase in tibial plateau SBP thickness in C57BL/6 mice (Huang et al., 2017). In humans, age-related changes in SBP thickness are inconsistent, with a decrease observed in femoral heads with age (Ries et al., 2020), no correlation observed in femoral heads with age (Nielsen et al., 2019), or increase in the talar dome with age (Nakasa et al., 2014). These SBP findings in age-related OA are limited, and the extent to which SBP thickness changes with cartilage degeneration with age is not well understood. These results motivate further investigation of SBP thickness with age. Given the association with SBP thickness and cartilage degeneration in injury and transgenic mouse models of OA (Jia et al., 2018; Bailey et al., 2021), we hypothesize that SBP thickens in the context of spontaneous age-related cartilage degeneration.

Taken together, these studies highlight the potential that osteocytes could represent a new cellular target for therapeutic intervention in joint disease and motivate the further study of osteocytes in human age-related OA. Tools such as high-throughput RNA sequencing (RNA-seq) offer an unbiased analysis of differentially expressed genes (DEGs) to identify candidate genes for further study, yet prioritization of these genes can be challenging without prior knowledge. We recently performed RNA-seq of aged osteocyte-enriched cortical bone from C57BL/6 mice and developed a computational mouse2human (M2H, www.mouse2human.org) gene set enrichment analysis pipeline to prioritize gene candidates based on association of variants in their human orthologs with clinically-relevant traits in genome wide association studies (GWAS). Using UK Biobank human fracture and bone mineral density GWAS of 426,824 individuals (Morris et al., 2019) M2H prioritized <1 % of the DEGs in aged mouse bone, including SOST, the target of the latest FDA-approved therapy for osteoporosis. Mouse age-related DEGs with unknown function in bone were also prioritized, based on their association with human fracture (Kaya et al., 2022), thus identifying new candidate genetic factors related to bone fracture. The goal of the current study is to prioritize analysis of clinically relevant genetic contributors to human OA identified among DEGs in aging mouse bone. We applied our M2H approach to human orthologs of mouse bone aging DEGs using the UK Biobank and Arthritis Research UK Osteoarthritis Genetics (arcOGEN) GWAS of human OA at multiple sites of joint degeneration (Tachmazidou et al., 2019).

2. Materials and methods

2.1. Animals

The role of aging on cartilage degeneration and SBP thickness was evaluated in male mice on a C57BL/6 background that possessed a floxed TβRII allele ($T\beta RII^{fl/fl}$). These mice do not express Cre and represent a "wild-type" phenotype (Dole et al., 2017; Dole et al., 2020). Left and right hindlimbs were collected at 6 months, 12 months, and 18 months of age for cartilage (n = 8–10 animals per group) and SBP (n = 4–5 animals per group) analysis, respectively. For RNA-seq analysis, wild-type male C57BL/6 mice were allowed to age to 2 months (2mo), 11 months (1y), 23 months (2y) and 30 months (2.5y) (n = 3 animals for 2mo; n = 4 animals for others) with well controlled conditions at the Buck Institute for Research on Aging. Tissues were collected from all mice simultaneously and RNA was isolated, as described (Kaya et al., 2022).

All animals were housed in groups in a pathogen-free facility at 22 °C with humidity range of 30–70 % and a 12-h light/dark cycle. Animals were supplied with standard irradiated mouse chow and water ad libitum. The Institutional Animal Care and Use Committee (IACUC) at the University of California San Francisco approved all animal studies.

2.2. Histology

Left hind limbs were sectioned at 6 μm thickness from paraffin-embedded knees at 90 degrees of flexion in the coronal orientation. Brightfield images were acquired on a Nikon Eclipse E800 microscope. For OA score, each joint quadrant (medial tibia, lateral tibia, medial femur, lateral femur) was imaged and graded by three blinded graders using modified Mankin grading schemes (n = 8–10 animals per group) (Furman et al., 2007; Mazur et al., 2019; Bailey et al., 2021). Scores from all graders were averaged to obtain a mean score, and mean scores were then averaged within each group. Total score represents the sum of all four quadrants, medial compartment score represents the sum of the medial femur and medial tibia, and lateral compartment score represents the sum of the lateral femur and lateral tibia.

2.3. MicroCT analysis

For SBP thickness analysis, right femoral condyles of the same mice were scanned using a Scanco μCT50 specimen scanner with an X-ray potential of 55 kVp, current of 109 μA, voxel size of 10 μm, and integration time of 500 milliseconds. Thresholding was performed as described (Dole et al., 2017; Fowler et al., 2017; Mazur et al., 2019; Bailey et al., 2021). The femoral SBP was contoured in a blinded manner in sagittal microCT images of the femoral condyles, and SBP thickness quantified in μm using grayscale 3D thickness maps (n = 4–5 animals per group), as described (Jia et al., 2018; Bailey et al., 2021). Figures contain pseudocolor images converted from representative grayscale images.

2.4. RNA isolation and sequencing

To yield RNA from aged mouse bone enriched for osteocytes, humeri were harvested, soft tissues, periosteum, and epiphyses were dissected, and bone marrow was removed by centrifugation, as described (Halleux et al., 2012; Kelly et al., 2014). Harvested bones were immediately snap-frozen in liquid nitrogen, and RNA was isolated, as previously described (Fowler et al., 2017; Mazur et al., 2019; Kaya et al., 2022). Isolated RNA samples that passed the Bioanalyzer quality control threshold of RNA Integrity Number > 7 were used for RNA library preparation using the Illumina TruSeq Stranded mRNA sample preparation kit with 500 ng of total RNA, according to manufacturer's protocol. An Illumina HiSeq 4000 at the UCSF Functional Genomics Core (San Francisco, CA) sequenced 50-bp single-end reads. Overall quality of the raw RNA sequencing reads was assessed using FastQC. Illumina single-end sequencing reads were uniquely aligned to the mouse reference genome (Ensembl, GRCm38.78) using STAR aligner (v. 2.5.2b) (Dobin et al., 2013). The RNA-seq data is available at the Sequence Read Archive (SRA) database of the National Center for Biotechnology Information (NCBI) under the BioProject PRJNA695408 (Kaya et al., 2022).

2.5. Mouse gene tables generated by RNA sequencing analysis

i) DEG tables from pairwise differential expression analysis: DEG tables for each of the three age comparison sets, 1y, 2y, and 2.5y mouse bone compared to 2 month old bone (2mo-1y, 2mo-2y and 2mo-2.5y), were generated for the M2H strategy for OA as in Kaya et al. (2022) (Kaya et al., 2022). Briefly, DESeq2 package (v.1.24.0) (Love et al., 2014) was

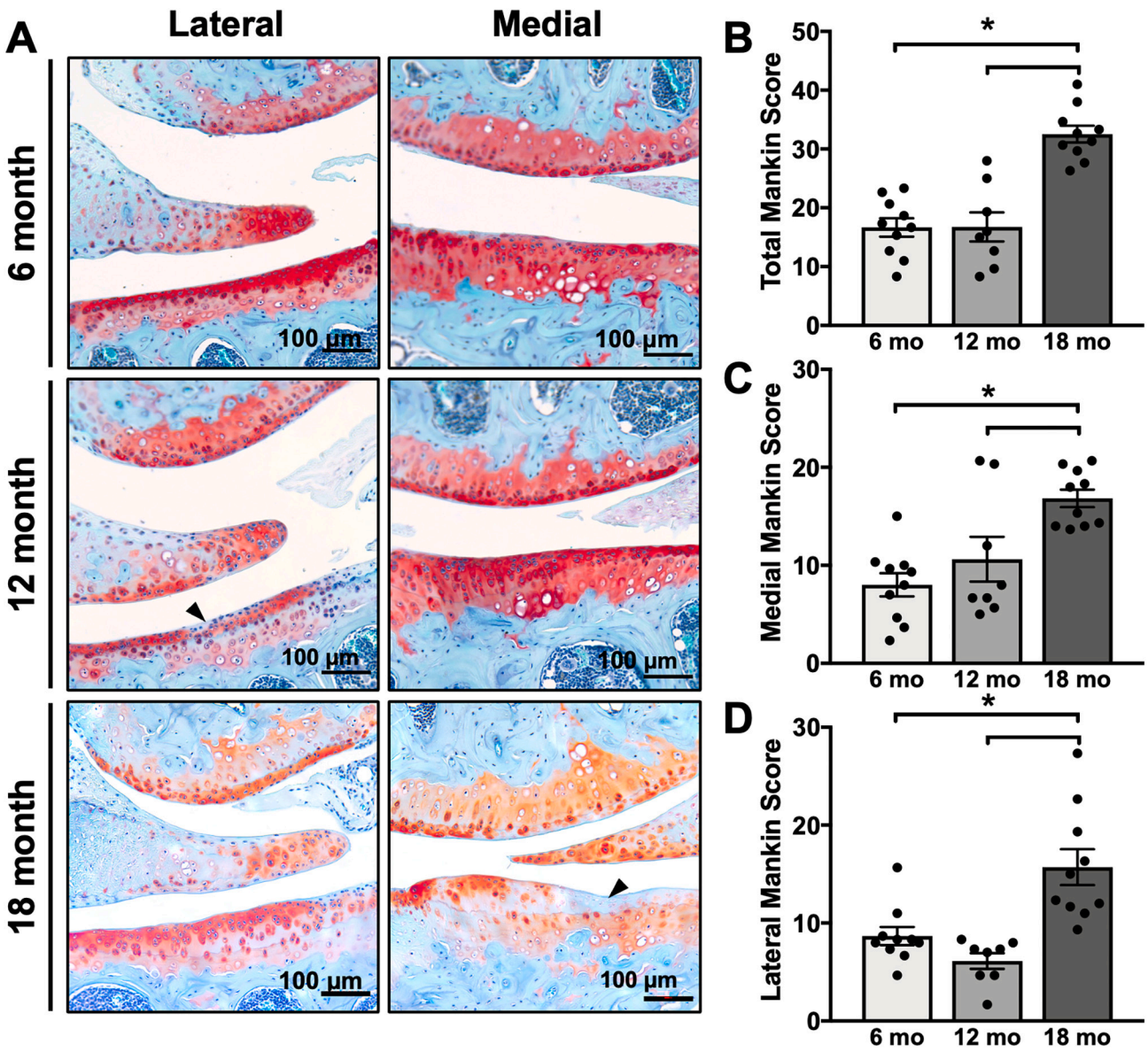

Fig. 1. Aging increases cartilage degeneration in the murine knee. 18-month-old male mice have significantly increased Mankin scores in the whole joint (B, n = 8–10 mice per group) and the medial and lateral joint compartments (C, D, n = 8–10 mice per genotype) when compared with 6- and 12-month-old mice (Safranin-O/Fast Green stain, A, scale bar = 100 μm). Arrows denote proteoglycan loss. Bar graphs represent mean ± SEM. *p < 0.05 between ages by one-way ANOVA and Tukey post-hoc test.

used to determine differentially expressed genes for 2mo-1y, 2mo-2y and 2mo-2.5y based on the Wald test. Significance criteria were set to the Benjamini-Hochberg (BH) false discovery rate (FDR) < 0.05.

ii) DEG tables from time course differential expression analysis: A likelihood ratio test (LRT) was performed to determine the genes with differences in their expression in any of the 4 time points (2 m, 1y, 2y, 2.5y) using DESeq2 package as previously reported (Kaya et al., 2022). DEGs with BH adjusted-*p* values (FDR) < 0.05 were considered significant. Nine different DEG clusters with similar gene expression patterns in 4 time points were generated by the *degPatterns* function in DEGreport package (1.30.0) in R using the hierarchical clustering method (Pantano, 2022). These 9 clusters of DEGs were used for the M2H strategy for OA, as previously described in application of M2H for BMD and fracture (Kaya et al., 2022).

iii) Pathway analysis: Over-representation analysis (ORA) was conducted to gain insight into the underlying biological processes in aging bone. Enriched Kyoto Encyclopedia of Genes and Genomes (KEGG) pathways were determined for nine clusters of DEGs identified by time course DE analysis using the *compareCluster* function in the clusterProfiler package (v.3.12.0) (Wu et al., 2021). Pathways with BH adjusted *p*-values smaller than 0.05 were significant.

2.6. Enrichment analysis of mouse DEGs using human UK Biobank and arcOGEN GWAS results

We used the previously published genome-wide association study results for OA which leveraged the UK Biobank and arcOGEN results. Genetic associations were available for approximately 17.5 million single-nucleotide variants in up to 455,221 individuals. Four phenotypes were analyzed in the GWAS: knee OA (24,955 cases), hip OA (15,704 cases), knee and/or hip OA (39,427 cases) and OA at any site (77,052 cases) with a total of 378,169 controls (Tachmazidou et al., 2019).

Gene set enrichment analysis was performed using DEGs (FDR < 0.05) from mouse RNA-seq and UK Biobank and arcOGEN GWAS results from four traits: hip, knee, hip and knee, and OA at any site, as described (Kaya et al., 2022). Briefly, MAGMA (v1.10) (de Leeuw et al., 2015) was

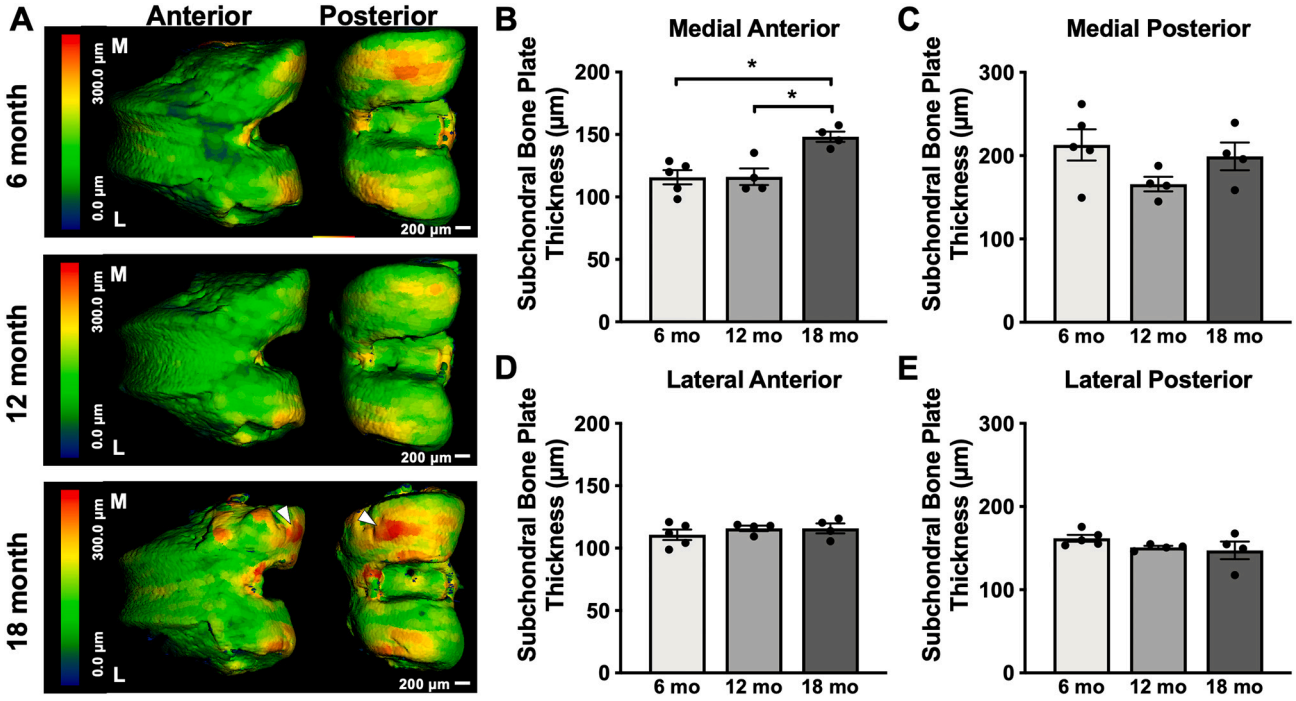

Fig. 2. Subchondral bone plate thickness increases with age in the murine femoral condyle. Femoral condyles from 18-month-old mice have spatial differences, denoted by white arrows, in subchondral bone plate (SBP) thickness compared with 6- and 12-month-old mice (microCT-derived thickness maps, A, scale bar = 200 µm), resulting in significantly higher SBP thickness in the anterior region of the medial femoral condyle (B, n = 4–5 mice per group). SBP thickness was not significantly different across age in any of the other regions evaluated (C, D, E, n = 4–5 mice per group). Bar graphs represent mean ± SEM. *p < 0.05 between ages by one-way ANOVA and Tukey post-hoc test.

used to calculate gene-based scores for each human ortholog of mouse genes using published human GWAS results for OA (Tachmazidou et al., 2019). Mouse to human homology was determined based on NCBI's Homologene resource from the file *HOM_MouseHumanSequence.rpt* which downloaded on 2020-04-28 (Human and mouse homology, 2020). Gene set enrichment analysis through MAGMA was then used to determine whether mouse DEGs harbor variants associated with hip OA, knee OA, knee and/or hip OA, and OA at any site.

i) Gene-based scores: MAGMA software (de Leeuw et al., 2015) was used to determine gene-based scores for each gene in the entire genome leveraging published GWAS results which provide single variant level information. A total of 100 kb non-coding gene region was identified (50 kb upstream and downstream of the gene region) and the most significant variant was selected to determine the gene-based score after adjusting for potential confounders, such as linkage disequilibrium between variants, gene density, and gene size (de Leeuw et al., 2015). Gene-based scores of all genes for OA traits are listed in www.mouse2human.org website.

ii) Gene set enrichment: In order to determine whether human orthologs of mouse DEG sets from either pairwise or time course DE analysis were enriched for associations with human knee OA, hip OA, knee and hip OA and OA at any site, MAGMA enrichment analysis was performed. MAGMA uses a one-sided enrichment test to determine whether gene-based scores for a set of DEGs are greater than all gene-based scores across the genome (de Leeuw et al., 2015). p value <0.05 was considered statistically significant. Once the gene set enrichment analysis was performed, the statistical significance of each gene-based score within the mouse DEG set was examined using the Bonferroni correction method. Significance criteria was set to adjusted-p value<0.05.

2.7. Statistical analysis

Comparisons across ages for murine OA development and SBP analysis employed one-way ANOVA followed by Tukey post-hoc tests, performed in GraphPad Prism 8 (GraphPad Software, Inc.). Values are expressed as mean ± SD for outcomes reporting a mean of individual measurements or ± SEM for outcomes reporting a mean of mean measurements. p values <0.05 were considered statistically significant, with sample size "n" specified in figure legends. Statistical outliers >3 SD from the mean were omitted (Dunn, 2021).

Multiple hypothesis testing correction was used in differential expression analysis of mouse RNA-seq (Benjamini-Hochberg), and gene-based score significance within a gene set (Bonferroni). Adjusted p values <0.05 were considered statistically significant. Gene-based association scores and gene set enrichment analysis were performed using MAGMA analysis software (v1.10, https://ctg.cncr.nl/software/magma). p values <0.05 were statistically significant.

We used *pwr.anova.test* function in pwr package in R (Champely, 2020) to detect power based on significance of 0.05 for histology and microCT studies. For a significance level = 0.05, effect size = 0.9, sample size = 8 mice/group, 96 % power was detected for histology. For the microCT, 96 % power was also detected for a significance level = 0.05, effect size = 1.4, sample size = 4 mice/group. We achieved 84 % power in our RNA-seq experiments with 50 depth coverage, 2 effect size, 0.29 coefficient of variation (cv) and 0.05 significance level by *rnapower* function in RNASeqPower package in R (Therneau et al., 2021).

3. Results

3.1. Subchondral bone plate thickness increases in the medial femoral condyle with age

Consistent with prior reports in C57BL/6 mice (Wilhelmi and Faust, 1976; Fang and Beier, 2014), aging male mice demonstrate age-related cartilage degeneration at 18 months of age (Fig. 1A). When compared with mice aged to 6 months and to 12 months, mice aged to 18 months show a significant increase in modified Mankin scores in the whole joint

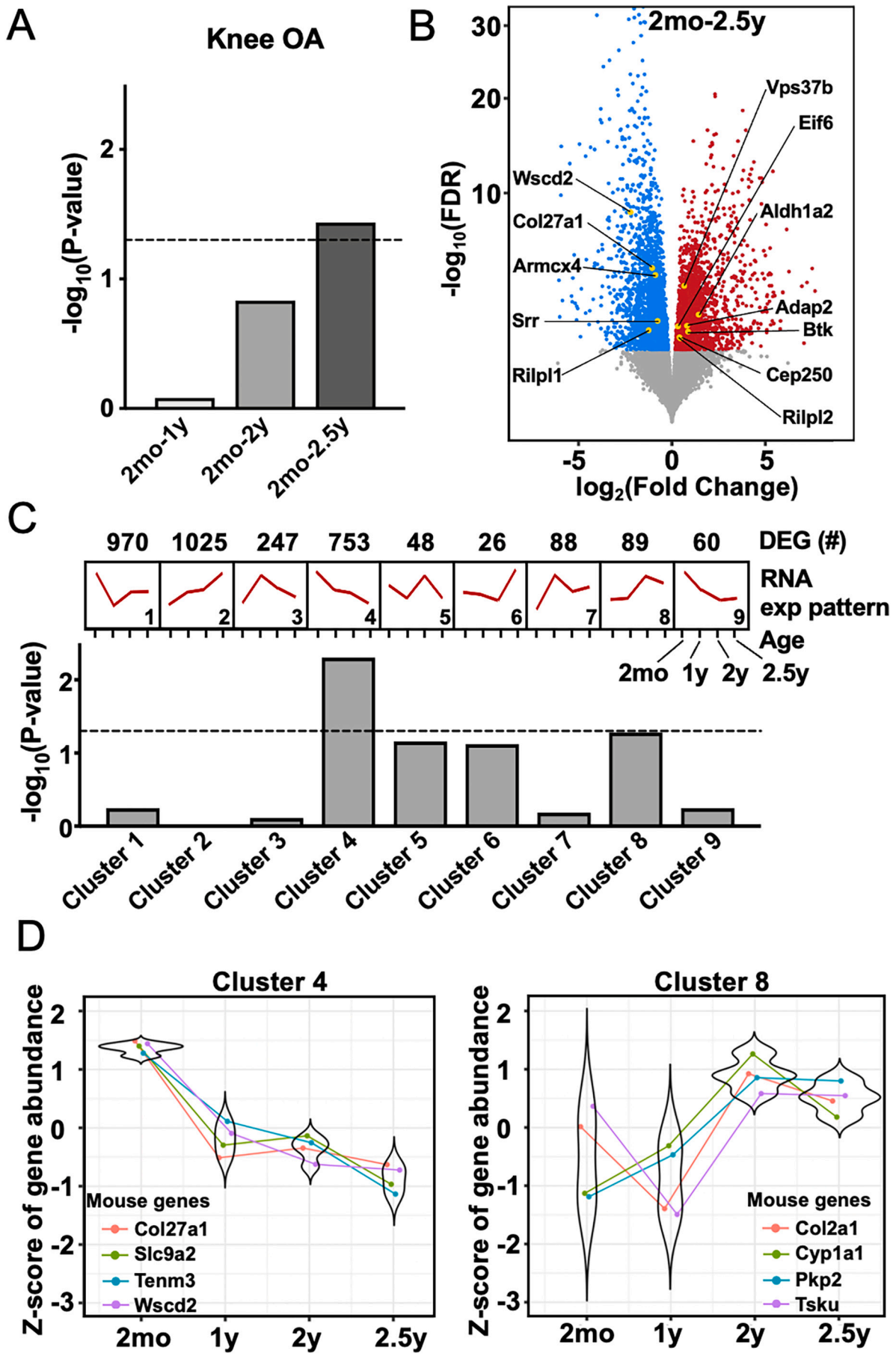

(caption on next page)

Fig. 3. Aging mouse bone differentially expressed genes (DEGs) are enriched for human genetic associations with knee osteoarthritis (OA). Mouse2human (M2H) enrichment analysis was performed using human orthologs of mouse RNA-seq DEGs identified by pairwise analysis (A,B), and by time course analysis (C,D) using GWAS of human knee osteoarthritis in the UK Biobank and arcOGEN. As shown by the dashed line significance threshold, the gene set for 2mo-2.5y is enriched for knee OA (A, $p < 0.05$). Twelve mouse genes out of 4195 DEGs in the oldest pairwise 2mo-2.5y group are significant (shown in gold, B, Bonferroni adjusted-$p < 0.05$). We previously reported 9 distinct patterns of mouse bone gene expression with age, as shown schematically in C, along with the number of DEGs in each cluster. Age-related clusters 4 and 8 are enriched for knee OA (C, $p < 0.05$). D shows the expression pattern for each of 4 genes that are significantly associated with human knee OA in each age-related clusters 4 and 8 (Bonferroni adjusted-$p < 0.05$).

and in the medial and lateral compartments ($p < 0.05$, Fig. 1B-D). No significant differences were observed between 6 and 12 months of age, consistent with prior literature (Wilhelmi and Faust, 1976, Fang and Beier, 2014).

In line with age-dependent cartilage degeneration observed in the aged mice, SBP thickness likewise increases by 18 months of age, when compared with mice aged to 6 months and to 12 months (Fig. 2). As with cartilage degeneration, no significant differences were observed between 6 and 12 months of age (Fig. 2B-E). Significant age-dependent differences in SBP thickness were observed only in the medial anterior compartment (Fig. 2A, B), with no significant differences in any of the other three quadrants.

3.2. Aging mouse bone DEGs are enriched for human genetic associations with knee OA

Given the age-related cartilage and subchondral bone changes in the murine knee, we sought to determine if male mouse genes that are differentially expressed in aging bone are enriched for association with human OA traits. We performed M2H gene set enrichment analysis for three DEG sets: 2mo-1y, 2mo-2y, and 2mo-2.5y with 1150, 1312 and 4195 DEGs, respectively, (FDR < 0.05) from pairwise analysis. Gene set enrichment analysis was also performed using nine DEG sets from clusters of genes identified by patterns of age-related changes across two month, one year, two years, and 2.5 years) (Kaya et al., 2022). The representative gene expression patterns for nine age-related clusters (2mo, 1y, 2y, 2.5y) are shown in Fig. 3C. Gene set enrichment analysis showed that sets of DEGs from the oldest 2mo-2.5y pairwise comparison, as well as from age-related clusters 4 and 8 were enriched for human knee OA ($p < 0.05$, Fig. 3A, C, Table 1). Genes in age-related cluster 8 have elevated expression at 2 and 2.5 years, especially relative to the 1-year time point, whereas genes in age-related cluster 4 are primarily downregulated with age.

Further, the M2H strategy was used to prioritize age-related changes in mouse bone gene expression, based on their clinical relevance to human OA. Among the 4195 mouse DEGs in 2mo-2.5y group, 12 genes were significantly associated with human knee OA after performing multiple test correction (Bonferroni, adjusted-$p < 0.05$, Fig. 3B, Supplemental Table S2). The 12 genes significantly associated with human knee OA are highlighted in gold on the volcano plot (Fig. 3B, Table 2), showing 2144 mouse bone genes that are repressed with age (blue, FDR < 0.05) and the 2051 genes that are induced with age (red, FDR < 0.05). Moreover, among the 753 and 89 DEGs in age-related clusters 4 and 8, only 4 genes for each cluster are significantly associated with knee OA (Bonferroni adjusted-$p < 0.05$, Supplemental Table S2). The temporal expression patterns of the human OA-associated genes from age-related cluster 4 (*Col27a1, Slc9a2, Tenm3, and Wscd2*) and cluster 8 (*Col2a1, Cyp1a1, Pkp2, and Tsku*) are shown in Fig. 3D. Of these, *Col27a1* and *Wscd2* also appeared as significant in 2mo-2.5y pairwise comparison table (Table 2).

3.3. Aging mouse bone DEGs are enriched for human genetic associations with hip OA

The M2H strategy was also applied to the same mouse DEG sets used for knee OA trait to determine if the mouse bone genes significantly associated with human knee OA differed among OA-affected joints using the published UK Biobank and arcOGEN GWAS for human hip OA (Tachmazidou et al., 2019). Unlike for knee OA, gene set enrichment analysis through MAGMA showed that 2mo-2y as well as age-related clusters 1 and 8 mouse DEG tables were enriched for the human hip OA ($p < 0.05$, Fig. 4A, C, Table 1). Gene-based scores identified 11 genes that are significantly enriched for human hip OA, highlighted in gold on the volcano plot of DEGs comparing 2mo-2y mouse bone (Fig. 4B, Supplemental Table S3). Of these, 10 genes are downregulated; only *Plekhm1* is upregulated with age. Gene-based scores for the enriched gene clusters identify 11 out of the 970 DEGs in age-related cluster 1 that are enriched for human hip OA (Fig. 4D, Supplemental Table S3). Among these, *Col11a1* and *Rgl1* were significantly associated with human hip OA both in the 2mo-2y and cluster 1 table (Table 2). Only one gene, *Atcay*, is significantly enriched for hip OA in age-related cluster 8, containing 89 DEGs (Fig. 4D).

3.4. Aging mouse bone DEGs are enriched for human genetic associations with knee-hip OA and OA at any site

Applying our M2H strategy to the published UK Biobank and arcOGEN GWAS phenotypes for human knee-hip OA and OA at any site, we find 2mo-2.5y and age-related cluster 4 were enriched for knee-hip OA ($p < 0.05$, Supplemental Table S1), whereas 2mo-1y and 2mo-2.5y groups and age-related clusters 1, 4, and 8 were enriched for OA at any site ($p < 0.05$, Supplemental Table S1). After correcting the gene-based *p* values, we identified 22 genes in 2mo-2.5y and 3 genes in age-related cluster 4 that are significantly enriched with human knee-hip OA (Bonferroni adjusted-$p < 0.05$; Supplemental Table S4). Eleven of these genes are shared in associations with each knee OA and hip OA, respectively. For OA at any site, we identified 14 genes in 2mo-1y, 25 genes in 2mo-2.5y, 15 genes in cluster 1, 7 genes in cluster 4, and 6 genes in cluster 8 that are significantly enriched (Bonferroni adjusted-$p < 0.05$; Supplemental Table S5).

3.5. DEGs with unique temporal expression patterns implicate distinct pathways

Our published over-representation analysis from aging mouse bone RNA-seq showed that the top 11 out of 15 significant KEGG pathways were shared for three pairwise age groups (2mo-1y, 2mo-2y, 2mo-2.5y) (Kaya et al., 2022). These results also highlight the induction of inflammatory and immunomodulatory pathways in the oldest 2mo-2.5y group, a pattern distinct from 2mo-1y and 2mo-2y groups. (Kaya et al., 2022). Performing pathway analysis of the up and down-regulated DEGs, separately at each time point, we found that inflammatory pathways were attributed to the upregulated genes for all age groups. We then performed KEGG pathway analysis for each of the nine clusters (Supplemental Fig. S1). Only age-related cluster 2, which is dominated by upregulated DEGs, has similar inflammatory pathways to those observed in pairwise analysis of upregulated DEGs with aging. Age-related clusters 1, 4, and 8, which were significantly associated with OA, did not enrich for inflammatory or disease related pathways (Supplemental Fig. S1, Supplemental Table S6).

3.6. Website: www.mouse2human.org

We previously created a browsable and interactive web-based tool: www.mouse2human.org based on UK Biobank GWAS of bone mineral density and fracture. In this study, we extended this website to the OA

Table 1
MAGMA UK Biobank and arcOGEN GWAS enrichment results for human knee and hip OA.

			Knee OA[c]		*Hip OA*[d]	
Aging gene sets	*Mouse DEGs*[a]	*No. of genes in MAGMA analysis*[b]	*MAGMA enrichment p value*[e]	*MAGMA significant genes*[f]	*MAGMA enrichment p value*[e]	*MAGMA significant genes*[f]
2mo – 1y	1151	963	0.829	2	*0.735*	8
2mo – 2y	1312	1083	0.147	4	**5×10^{-3} ***	**11**
2mo – 2.5y	4195	3499	**0.037** *	**12**	0.083	29
Cluster 1	970	898	0.567	1	**5×10^{-3} ***	**11**
Cluster 2	1025	747	0.990	4	0.562	5
Cluster 3	247	213	0.778	3	0.922	0
Cluster 4	753	682	**5×10^{-3} ***	**4**	0.276	8
Cluster 5	48	40	0.069	0	0.533	1
Cluster 6	26	19	0.075	2	0.957	1
Cluster 7	88	55	0.654	0	0.492	1
Cluster 8	89	60	**0.052** *	**4**	**0.040** *	**1**
Cluster 9	60	49	0.565	0	0.570	0

[a] Number of differentially expressed genes (DEGs) from mouse RNA-seq analysis (FDR < 0.05) (Kaya et al., 2022).
[b] Not all mouse DEGs have human homologs or gene-based GWAS scores.
[c] Published UK Biobank and arcOGEN GWAS results for knee OA.
[d] Published UK Biobank and arcOGEN GWAS results for hip OA.
[e] MAGMA enrichment analysis. Significantly enriched gene sets are in **bold** *: $p < 0.05$.
[f] Bonferroni correction is applied for each gene for each aging gene set. Significance level: adjusted-$p < 0.05$.

GWAS of knee OA, hip OA, knee and hip OA, and OA at any site. Using the same gene-based scoring described in the Methods, users can evaluate any mouse or human gene for its association with human OA in the UK Biobank and arcOGEN (Tachmazidou et al., 2019). Additionally, a group of genes can be searched together using the batch query tab and their adjusted-p values for multiple testing will be obtained using both Bonferroni and Benjamini-Hochberg (BH) FDR methods. Users can also run their custom gene set enrichment analysis using the code provided in the code tab on the website, since this is too computationally intensive to reliably operate on the website.

4. Discussion

Disruption of subchondral bone is a well-known phenotype in OA development (Burr and Gallant, 2012; Goldring and Goldring, 2016), and recently the role of SBP thickness in OA was linked with osteocyte dysfunction (Bailey et al., 2021). Moreover, subchondral bone from patients with knee OA showed severely impaired osteocyte activity with hallmarks of PLR suppression, and mice with osteocyte-intrinsic defects in the PLR enzyme MMP13 yielded an early OA phenotype with PLR suppression in the subchondral bone and disruption of cartilage homeostasis (Mazur et al., 2019). The role of SBP thickness and osteocytes in age-related OA, however, was less understood. In a recent study, aging mice exhibit repression of osteocytic TβRII expression and LCN degeneration, raising the possibility that defective osteocyte function may contribute to age-related OA (Schurman et al., 2021). Using a mouse model of age-related OA and unbiased analyses of large-scale mouse transcriptomic and human GWAS data, we observe SBP thickening coinciding with cartilage degeneration and identify novel DEGs in aging mouse bone associated with human knee OA and hip OA. The impact of this study is to provide prioritized differentially expressed genes in aging mouse bone that predict clinically relevant OA outcomes, and ultimately identify novel genes as potential targets for OA diagnostics and therapies. Although this study is limited in its ability to demonstrate a causal relationship between osteocyte dysfunction and SBP changes in age-related OA, the M2H approach is used as a utility, and the findings from this work support a role for osteocytes in the development of OA through bone-cartilage crosstalk. In combination with prior work demonstrating that osteocytes play a key role in the pathogenesis of OA, we hypothesize that this is likewise true in aging bone.

Even though changes with subchondral bone are well known to occur in parallel with cartilage degeneration (Burr and Gallant, 2012, Goldring and Goldring, 2016), there remain questions about the sequence and drivers of joint degeneration. This work provides further evidence of concurrent degeneration yet does not tease apart the causality of bone changes to cartilage degeneration or vice versa. More specifically, we find a significant increase in SBP thickness in 18-month-old C57BL/6 mice. Thickening occurs in the medial anterior compartment, a relatively unloaded portion of the joint, whereas cartilage degeneration occurs on both the medial and lateral side of the joint in a relatively loaded portion of the joint. The uncoupling of cartilage degeneration and SBP thickening in the loaded region of the joint raises the possibility that other factors may be contributing to cartilage degeneration. First, thickening of bone in the medial anterior compartment may cause qualitative changes in joint shape and joint biomechanics in the other compartments not captured in our analyses. Second, the relationship between SBP thickness and cartilage degeneration may differ in age-related OA versus that observed with trauma or injury (Jia et al., 2018; Bailey et al., 2021). Distinct sequential changes in bone and cartilage degeneration have previously been reported for different etiologies of OA (Burr and Gallant, 2012; Goldring and Goldring, 2016; Sacitharan and Vincent, 2016).

Defects in osteocyte function cause a host of changes in subchondral bone and can play a causal role in OA. However, the mechanisms by which osteocyte dysfunction contributes to cartilage degeneration, or might be modifiable to prevent OA, are unclear. For example, LCN degeneration in aged bone or bone deficient in TβRII is sufficient to explain the impaired mechanosensitivity in each model (Meakin et al., 2014; Chermside-Scabbo et al., 2020; Schurman et al., 2021), and loss of osteocytic TβRII coincides with deregulation of the mechanosensitive protein Sclerostin and SBP thickening (Bailey et al., 2021). Additionally, bone shape is a strong predictor of OA (Lynch et al., 2009; Bredbenner et al., 2010; Baker-Lepain et al., 2012; Neogi et al., 2013; Morales Martinez et al., 2020), and our recent work supports a role for osteocytes in the control of bone shape (Bailey et al., 2021). Further research is needed to quantitatively assess the changes in subchondral bone shape in mice that acquire OA with age or with osteocyte-intrinsic defects.

M2H provides new insights while reinforcing conclusions derived from traditional GWAS, including the genetic evidence for distinct mechanisms driving knee OA and hip OA in humans (Hall et al., 2022). M2H was used to analyze 12 DEG sets (three from pairwise comparison age groups and nine clusters from time course analysis) from mouse cortical bone RNA-seq (Kaya et al., 2022) using the UK Biobank and arcOGEN OA GWAS (Tachmazidou et al., 2019). Different DEG sets uniquely enriched for human knee OA or hip OA, such that age-related

Table 2
MAGMA-identified aging mouse bone DEGs associated with human knee and hip OA using UK Biobank and arcOGEN GWAS results for pairwise comparison age groups of 2mo-2y (2y) and 2mo-2.5y (2.5y), and clusters 1, 4 and 8. Common genes in both gene sets are in bold.

Human	Human		Mouse			Mouse2human (M2H)		Mouse
OA trait	*Gene ID*	*Entrez ID*	*Gene ID*	*Entrez ID*	*Gene set tables*	*MAGMA gene-based p value*[a]	*Adjusted p value*[b]	Gene expression[c]
Knee	ADAP2	55803	Adap2	216991	2.5y	9.6×10^{-6}	0.034	Up
Knee	ALDH1A2	8854	Aldh1a2	19378	2.5y	1.1×10^{-6}	4.0×10^{-3}	Up
Knee	ARMCX4	100131755	Armcx4	100503043	2.5y	1.4×10^{-5}	0.048	Down
Knee	BTK	695	Btk	12229	2.5y	9.2×10^{-6}	0.032	Up
Knee	CEP250	11190	Cep250	16328	2.5y	1.4×10^{-22}	5.0×10^{-19}	Up
Knee	**COL27A1**	**85301**	**Col27a1**	**373864**	**2.5y**	$\mathbf{2.3 \times 10^{-7}}$	$\mathbf{1.6 \times 10^{-4}}$	**Down**
Knee	**COL27A1**	**85301**	**Col27a1**	**373864**	**Cluster4**	$\mathbf{2.3 \times 10^{-7}}$	$\mathbf{8.2 \times 10^{-4}}$	–
Knee	COL2A1	1280	Col2a1	12824	Cluster 8	2.7×10^{-4}	0.016	–
Knee	CYP1A1	1543	Cyp1a1	13076	Cluster 8	3.5×10^{-5}	2.1×10^{-3}	–
Knee	EIF6	3692	Eif6	16418	2.5y	8.0×10^{-18}	2.8×10^{-14}	Up
Knee	PKP2	5318	Pkp2	67451	Cluster 8	3.5×10^{-4}	0.021	–
Knee	RILPL1	353116	Rilpl1	75695	2.5y	8.8×10^{-7}	3.1×10^{-3}	Down
Knee	RILPL2	196383	Rilpl2	80291	2.5y	1.2×10^{-7}	4.3×10^{-4}	Up
Knee	SLC9A2	6549	Slc9a2	226999	Cluster 4	1.8×10^{-5}	0.012	–
Knee	SRR	63826	Srr	27364	2.5y	2.3×10^{-6}	8.2×10^{-3}	Down
Knee	TENM3	55714	Tenm3	23965	Cluster 4	1.8×10^{-5}	0.012	–
Knee	TSKU	25987	Tsku	244152	Cluster 8	3.8×10^{-4}	0.022	–
Knee	VPS37B	79720	Vps37b	330192	2.5y	9.7×10^{-7}	3.4×10^{-3}	Up
Knee	**WSCD2**	**9671**	**Wscd2**	**320916**	**2.5y**	$\mathbf{4.4 \times 10^{-6}}$	**0.0156**	**Down**
Knee	**WSCD2**	**9671**	**Wscd2**	**320916**	**Cluster 4**	$\mathbf{4.4 \times 10^{-6}}$	**0.003**	**–**
Hip	ATCAY	85300	Atcay	16467	Cluster 8	8.6×10^{-4}	0.051	–
Hip	BMP5	653	Bmp5	12160	2y	3.7×10^{-6}	4.2×10^{-3}	Down
Hip	BRSK1	84446	Brsk1	381979	2y	2.0×10^{-5}	0.022	Down
Hip	CFAP251	144406	Wdr66	269701	2y	4.5×10^{-6}	4.8×10^{-3}	Down
Hip	**COL11A1**	**1301**	**Col11a1**	**12814**	**2y**	$\mathbf{8.4 \times 10^{-14}}$	$\mathbf{9.2 \times 10^{-11}}$	**Down**
Hip	**COL11A1**	**1301**	**Col11a1**	**12814**	**Cluster 1**	$\mathbf{8.4 \times 10^{-14}}$	$\mathbf{7.6 \times 10^{-11}}$	**–**
Hip	DNAH1	25981	Dnah1	110084	2y	1.2×10^{-8}	1.3×10^{-5}	Down
Hip	**ECM1**	**1893**	**Ecm1**	**13601**	**2y**	$\mathbf{1.4 \times 10^{-5}}$	**0.015**	**Down**
Hip	**ECM1**	**1893**	**Ecm1**	**13601**	**Cluster 1**	$\mathbf{1.4 \times 10^{-5}}$	**0.012**	**–**
Hip	FGFR3	2261	Fgfr3	14184	Cluster 4	3.9×10^{-6}	3.6×10^{-3}	–
Hip	GLT8D1	55830	Glt8d1	76485	Cluster 4	3.6×10^{-11}	3.2×10^{-8}	–
Hip	LMX1B	4010	Lmx1b	16917	2y	3.3×10^{-9}	3.6×10^{-6}	Down
Hip	LRFN4	78999	Lrfn4	225875	Cluster 4	1.1×10^{-5}	0.010	–
Hip	LRIG3	121227	Lrig3	320398	2y	1.1×10^{-6}	1.2×10^{-3}	Down
Hip	MYO6	4646	Myo6	17920	Cluster 1	1.2×10^{-10}	1.1×10^{-7}	–
Hip	PLEKHM1	9842	Plekhm1	353047	2y	7.3×10^{-8}	7.9×10^{-5}	Up
Hip	**RGL1**	**23179**	**Rgl1**	**19731**	**2y**	$\mathbf{3.7 \times 10^{-7}}$	$\mathbf{4.0 \times 10^{-4}}$	**Down**
Hip	**RGL1**	**23179**	**Rgl1**	**19731**	**Cluster 1**	$\mathbf{3.7 \times 10^{-7}}$	$\mathbf{3.3 \times 10^{-4}}$	**–**
Hip	RUNX2	860	Runx2	12393	Cluster 1	2.1×10^{-12}	1.9×10^{-9}	–
Hip	SEMA3G	56920	Sema3g	218877	2y	2.3×10^{-10}	2.5×10^{-7}	Down
Hip	SPTBN2	6712	Sptbn2	20743	Cluster 1	4.0×10^{-6}	3.6×10^{-3}	–
Hip	TNC	3371	Tnc	21923	Cluster 1	9.5×10^{-9}	8.5×10^{-6}	–
Hip	TRIM32	22954	Trim32	69807	Cluster 1	2.2×10^{-9}	1.9×10^{-6}	–

[a] MAGMA gene-based score based on empirical min *p* value (Supplemental Table S2, S3).
[b] Multiple testing correction for each mouse DEG using Bonferroni correction method. Significance level: adjusted-p < 0.05 (Supplemental Table S2, S3).
[c] Gene expression levels from mouse RNA-seq: down = gene expression is downregulated for old animals compared to the young ones (2y vs 2mo) up = vice-versa (Kaya et al., 2022).

clusters 4 and 8, and the 2 m-2.5y DEG sets were significantly associated with knee OA, whereas age-related clusters 1 and 8, and the 2 m-2y DEG set were significantly associated with hip OA. Although using gene expression data from 30-month-old male mice could be seen as a limitation because of the influence of late-life disease (Yuan et al., 2009), DEGs in the OA associated age-related clusters (1, 4 and 8) do not show 30 month-specific gene expression changes. Though M2H used the same cluster sets, the significantly enriched clusters are different depending on OA site and none of the significant genes are shared between knee OA and hip OA. Pathway analysis reveals that inflammatory pathways are associated with upregulated genes for all age groups. Age-related cluster 8 has partially upregulated genes and is significantly enriched for knee and hip OA, consistent with the known inflammatory and immune component of this disease. Lastly, though cluster 8 is the only gene set containing <100 genes (others have >700), it is the only cluster enriched for both knee and hip OA, indicating the significance and relevance of these genes even though they are fewer.

Among the genes with previously-identified associations with human OA, the M2H approach prioritizes genes based on their differential expression in aging bone. While the role of some of these genes is well-established, the functional role of many, in bone or in OA, remains to be determined. Eighteen and 20 genes associated with knee OA and hip OA, respectively, were reported previously based on prior OA GWAS (Styrkarsdottir et al., 2018; Tachmazidou et al., 2019; Boer et al., 2021; Aubourg et al., 2022). Among these genes, we identified *Runx2* (hip OA), a key transcription factor controlling osteoblasts and chondrocyte differentiation, *Col11a1* (hip OA) and *Col2a1* (knee OA) and *Col27a1* (knee OA), which encode extracellular matrix proteins and are essential for collagen formation, and *Bmp5* (hip OA) and *Fgfr3* (Hip OA), which participate in BMP and FGF signaling pathways, each with well-known roles in OA development and skeletal abnormalities (Rodriguez et al., 2004; Jenkins et al., 2005; Deng et al., 2016; Okura et al., 2018; Chen et al., 2020; Shao et al., 2021). Furthermore, retinoic acid regulatory gene *Aldh1a2* (knee OA) was prioritized in our analyses, which is associated with severe hand OA in a previous GWAS (Styrkarsdottir et al., 2014), and its expression declines in OA cartilage (Shepherd et al., 2018). Ten of the 38 knee OA and hip OA associated genes (*Col11a1, Col27a1, Col2a1, Fgfr3, Lrig3, Sema3g, Slc9a2, Tnc, Tsku, Wscd2*) are

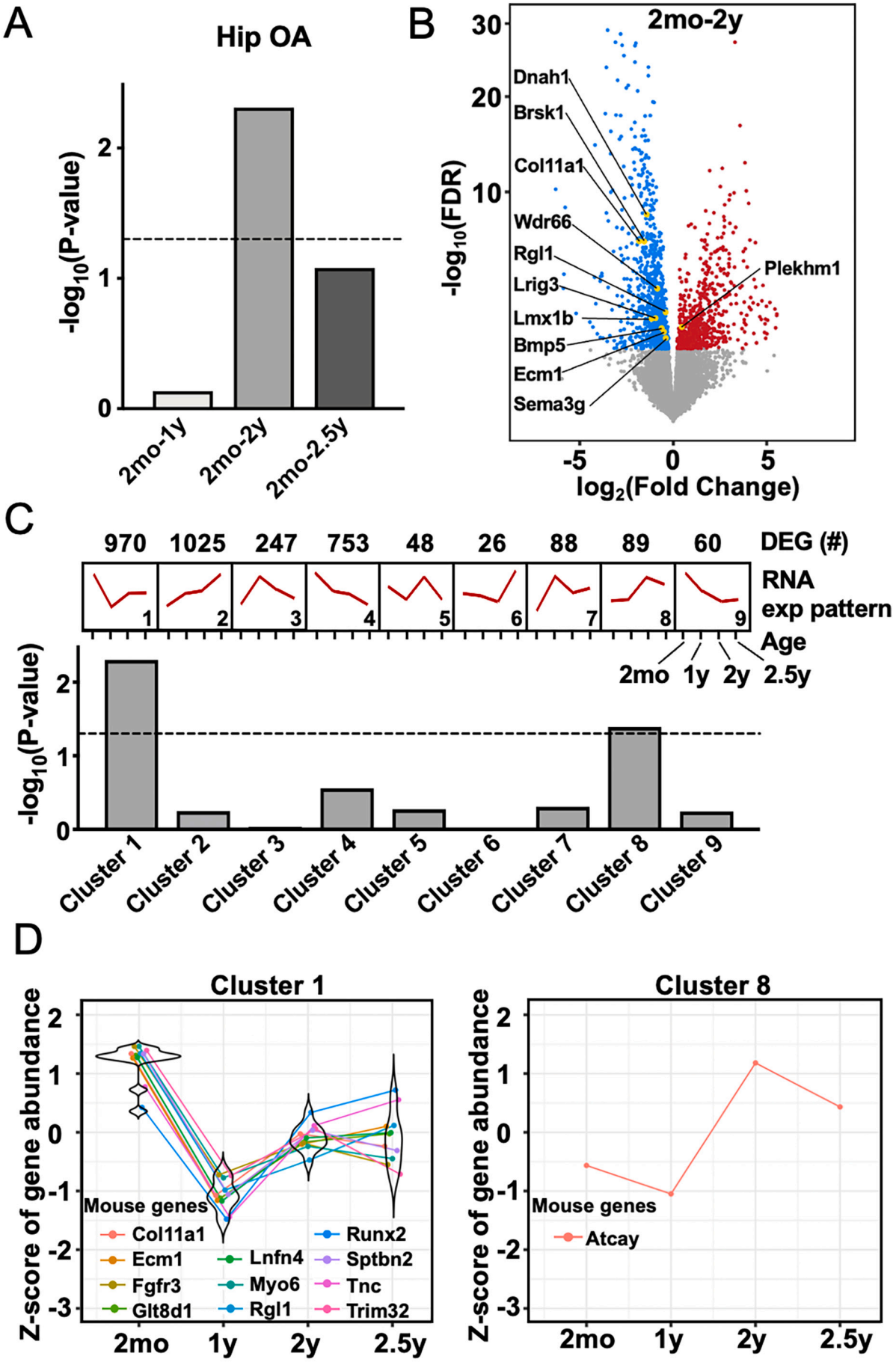

(caption on next page)

Fig. 4. Aging mouse bone differentially expressed genes (DEGs) are enriched for human genetic associations with hip osteoarthritis (OA). Mouse2human (M2H) enrichment analysis was performed using human orthologs of mouse RNA-seq DEGs identified by pairwise analysis (A,B) and by time course analysis (C,D) using GWAS of human hip osteoarthritis in the UK Biobank and arcOGEN. As shown by the dashed line significance threshold, the gene set for 2mo-2y is enriched for hip OA (A, $p < 0.05$). Eleven mouse genes out of 1312 DEGs in the pairwise 2mo-2y group are significant (shown in gold, B, Bonferroni adjusted-$p < 0.05$). We previously reported 9 distinct patterns of mouse bone gene expression with age, as shown schematically in C, along with the number of DEGs in each cluster. Age-related clusters 1 and 8 are enriched for hip OA (C, $p < 0.05$). D shows the expression pattern for 11 and 1 gene that are significantly associated with human hip OA in each age-related clusters 1 and 8 (Bonferroni adjusted-$p < 0.05$).

identified as osteocyte transcriptome signature genes (Youlten et al., 2021). Among these, *Tsku* (knee OA) can be further prioritized based on its role in regulating Wnt and TGFβ signaling pathways (Niimori et al., 2012), and *Lrig3* (hip OA) can be prioritized based on its role in regulating BMP signaling (Herdenberg et al., 2021). *Ecm1* (hip OA), *Rgl1* (hip OA) and *Wscd2* (knee OA) were prioritized in both pairwise (down-regulated) and cluster analysis (Table 2). *Wscd2* is of particular interest as one of the osteocyte transcriptome genes (Youlten et al., 2021). Of importance for studying the role of bone shape in OA, one of the variants within *Glt8d1* is associated with hip OA by changing proximal femur shape (Lindner et al., 2015). *Plekhm1* is essential for vesicular transport in osteoclasts and is associated with osteopetrosis and abnormal bone mineralization (Van Wesenbeeck et al., 2007). Lastly, mutations in *Lmx1b* are associated with limb dysplasia in nail-patella syndrome (McIntosh et al., 1998; Dreyer et al., 2000). Therefore, in light of their role in bone and their association with knee OA and hip OA, M2H prioritization of these genes motivates further mechanistic study of Tsku, Lrig3, and Wscd2, Glt8d1, Plekhm1 and Lmx1b in OA.

Given the technical limitations of obtaining mRNA from murine bone due to size, RNA-seq data presented from our aging mice represents age-dependent differentially regulated genes across whole humeri. Therefore, these RNA-seq findings suggest an overall age-related change in bone gene expression and limit our understanding of the spatial changes detected across the joint. Additionally, our SBP thickness maps highlight qualitative spatial changes, yet more rigorous shape modeling is needed to uncover quantitative changes in joint shape in our aging mouse model. Although there is a higher prevalence of OA in women (Tschon et al., 2021), the current study investigates the role of subchondral bone in the development of age-related OA in male mice. Given evidence of sex-dependent differences in osteocytic function in female mice (Dole et al., 2020) and the sex-specific role of osteocyte dysfunction in OA development (Bailey et al., 2021), further research is needed to fully uncover the role of osteocytes in age-related OA in female mice.

Taken together, these findings provide new evidence about the role of subchondral bone, and specifically osteocytes, in the development of joint degeneration with age. In mice, we find age-related changes in SBP thickness that coincide with cartilage degeneration. Further, we prioritize genes in mouse bone enriched for osteocytes that are differentially expressed with age using an unbiased M2H approach to identify human homologs containing genetic variants associated with OA. Given osteocytes have recently been identified as causal contributors to joint degeneration (Mazur et al., 2019; Bailey et al., 2021), identifying genetic contributors to OA in bone could motivate further mechanistic study and potential treatments for OA.

Supplementary data to this article can be found online at https://doi.org/10.1016/j.bonr.2022.101647.

Data availability

The RNA-seq data is available at the Sequence Read Archive (SRA) database of the National Center for Biotechnology Information (NCBI) under the BioProject PRJNA695408.

Acknowledgements

This research was supported by the National Institute of Dental and Craniofacial Research (R01 DE019284), the National Institute on Aging (U24AG051129), NRSA Individual Predoctoral Fellowship (F31AG063402), the Department of Defense (OR130191), UCSF Program for Breakthrough Biomedical Research, the Read Research Foundation, and the National Institute of General Medical Sciences (T32GM007618), and the UCSF Health Innovation via Engineering Postdoctoral Fellows Program (HIVE). The authors gratefully acknowledge Cristal Yee for assistance with tissue harvest and preparation, Courtney Mazur and Jennifer Salinas for assistance with histological analysis and Natalia Castillo for assistance with the literature search.

References

2020 Human and mouse homology classes with sequence information. http://www.informatics.jax.org/downloads/reports/index.html#homology, 2020.
Aubourg, G., Rice, S.J., Bruce-Wootton, P., Loughlin, J., 2022. Genetics of osteoarthritis. Osteoarthr. Cartil. 30 (5), 636–649.
Bailey, K.N., Nguyen, J., Yee, C.S., Dole, N.S., Dang, A., Alliston, T., 2021. Mechanosensitive control of articular cartilage and subchondral bone homeostasis in mice requires osteocytic transforming growth factor beta signaling. Arthritis Rheumatol. 73 (3), 414–425.
Baker-Lepain, J.C., Lynch, J.A., Parimi, N., McCulloch, C.E., Nevitt, M.C., Corr, M., Lane, N.E., 2012. Variant alleles of the wnt antagonist FRZB are determinants of hip shape and modify the relationship between hip shape and osteoarthritis. Arthritis Rheum. 64 (5), 1457–1465.
Boer, C.G., Hatzikotoulas, K., Southam, L., Stefansdottir, L., Zhang, Y., de Almeida, R. Coutinho, Wu, T.T., Zheng, J., Hartley, A., Teder-Laving, M., Skogholt, A.H., Terao, C., Zengini, E., Alexiadis, G., Barysenka, A., Bjornsdottir, G., Gabrielsen, M.E., Gilly, A., Ingvarsson, T., Johnsen, M.B., Jonsson, H., Kloppenburg, M., Luetge, A., Lund, S.H., Magi, R., Mangino, M., Nelissen, R., Shivakumar, M., Steinberg, J., Takuwa, H., Thomas, L.F., Tuerlings, M., Arc, O.C., Pain, H.A.-I., , A. Consortium, C. Regeneron Genetics, Babis, G.C., Cheung, J.P.Y., Kang, J.H., Kraft, P., Lietman, S.A., Samartzis, D., Slagboom, P.E., Stefansson, K., Thorsteinsdottir, U., Tobias, J.H., Uitterlinden, A.G., Winsvold, B., Zwart, J.A., Smith, G.Davey, Sham, P.C., Thorleifsson, G., Gaunt, T.R., Morris, A.P., Valdes, A.M., Tsezou, A., Cheah, K.S.E., Ikegawa, S., Hveem, K., Esko, T., Wilkinson, J.M., Meulenbelt, I., Lee, M.T.M., van Meurs, J.B.J., Styrkarsdottir, U., Zeggini, E., 2021. Deciphering osteoarthritis genetics across 826,690 individuals from 9 populations. Cell 184 (18), 4784–4818 e17.
Bonewald, L.F., 2011. The amazing osteocyte. J. Bone Miner. Res. 26 (2), 229–238.
Bredbenner, T.L., Eliason, T.D., Potter, R.S., Mason, R.L., Havill, L.M., Nicolella, D.P., 2010. Statistical shape modeling describes variation in tibia and femur surface geometry between control and incidence groups from the osteoarthritis initiative database. J. Biomech. 43 (9), 1780–1786.
Burr, D.B., Gallant, M.A., 2012. Bone remodelling in osteoarthritis. Nat. Rev. Rheumatol. 8 (11), 665–673.
Champely, S., 2020. pwr: basic functions for power analysis. https://CRAN.R-project.org/package=pwr.
Chen, D., Kim, D.J., Shen, J., Zou, Z., O'Keefe, R.J., 2020. Runx2 plays a central role in osteoarthritis development. J. Orthop. Transl. 23, 132–139.
Chermside-Scabbo, C.J., Harris, T.L., Brodt, M.D., Braenne, I., Zhang, B., Farber, C.R., Silva, M.J., 2020. Old mice have less transcriptional activation but similar periosteal cell proliferation compared to young-adult mice in response to in vivo mechanical loading. J. Bone Miner. Res. 35 (9), 1751–1764.
de Leeuw, C.A., Mooij, J.M., Heskes, T., Posthuma, D., 2015. MAGMA: generalized gene-set analysis of GWAS data. PLoS Comput. Biol. 11 (4), e1004219.
Deng, H., Huang, X., Yuan, L., 2016. Molecular genetics of the COL2A1-related disorders. Mutat. Res. Rev. Mutat. Res. 768, 1–13.
Dobin, A., Davis, C.A., Schlesinger, F., Drenkow, J., Zaleski, C., Jha, S., Batut, P., Chaisson, M., Gingeras, T.R., 2013. STAR: ultrafast universal RNA-seq aligner. Bioinformatics 29 (1), 15–21.
Dole, N.S., Mazur, C.M., Acevedo, C., Lopez, J.P., Monteiro, D.A., Fowler, T.W., Gludovatz, B., Walsh, F., Regan, J.N., Messina, S., Evans, D.S., Lang, T.F., Zhang, B., Ritchie, R.O., Mohammad, K.S., Alliston, T., 2017. Osteocyte-intrinsic TGF-beta signaling regulates bone quality through Perilacunar/Canalicular remodeling. Cell Rep. 21 (9), 2585–2596.
Dole, N.S., Yee, C.S., Mazur, C.M., Acevedo, C., Alliston, T., 2020. TGFbeta regulation of Perilacunar/Canalicular remodeling is sexually dimorphic. J. Bone Miner. Res. 35 (8), 1549–1561.
Dreyer, S.D., Morello, R., German, M.S., Zabel, B., Winterpacht, A., Lunstrum, G.P., Horton, W.A., Oberg, K.C., Lee, B., 2000. LMX1B transactivation and expression in nail-patella syndrome. Hum. Mol. Genet. 9 (7), 1067–1074.

Dunn, P.K., 2021. In: Scientific Research and Methodology: An Introduction to Quantitative Research and Statistics in Science, Engineering and Health, pp. 201–206. https://bookdown.org/pkaldunn/Book.
Fang, H., Beier, F., 2014. Mouse models of osteoarthritis: modelling risk factors and assessing outcomes. Nat. Rev. Rheumatol. 10 (7), 413–421.
Fowler, T.W., Acevedo, C., Mazur, C.M., Hall-Glenn, F., Fields, A.J., Bale, H.A., Ritchie, R.O., Lotz, J.C., Vail, T.P., Alliston, T., 2017. Glucocorticoid suppression of osteocyte perilacunar remodeling is associated with subchondral bone degeneration in osteonecrosis. Sci. Rep. 7, 44618.
Furman, B.D., Strand, J., Hembree, W.C., Ward, B.D., Guilak, F., Olson, S.A., 2007. Joint degeneration following closed intraarticular fracture in the mouse knee: a model of posttraumatic arthritis. J. Orthop. Res. 25 (5), 578–592.
Goldring, S.R., Goldring, M.B., 2016. Changes in the osteochondral unit during osteoarthritis: structure, function and cartilage-bone crosstalk. Nat. Rev. Rheumatol. 12 (11), 632–644.
Hall, M., van der Esch, M., Hinman, R.S., Peat, G., de Zwart, A., Quicke, J.G., Runhaar, J., Knoop, J., van der Leeden, M., de Rooij, M., Meulenbelt, I., Vliet Vlieland, T., Lems, W.F., Holden, M.A., Foster, N.E., Bennell, K.L., 2022. How does hip osteoarthritis differ from knee osteoarthritis? Osteoarthr. Cartil. 30 (1), 32–41.
Halleux, C., Kramer, I., Allard, C., Kneissel, M., 2012. Isolation of mouse osteocytes using cell fractionation for gene expression analysis. Methods Mol. Biol. 816, 55–66.
Herdenberg, C., Mutie, P.M., Billing, O., Abdullah, A., Strawbridge, R.J., Dahlman, I., Tuck, S., Holmlund, C., Arner, P., Henriksson, R., Franks, P.W., Hedman, H., 2021. LRIG proteins regulate lipid metabolism via BMP signaling and affect the risk of type 2 diabetes. Commun. Biol. 4 (1), 90.
Huang, H., Skelly, J.D., Ayers, D.C., Song, J., 2017. Age-dependent changes in the articular cartilage and subchondral bone of C57BL/6 mice after surgical destabilization of medial meniscus. Sci. Rep. 7, 42294.
Jenkins, E., Moss, J.B., Pace, J.M., Bridgewater, L.C., 2005. The new collagen gene COL27A1 contains SOX9-responsive enhancer elements. Matrix Biol. 24 (3), 177–184.
Jia, H., Ma, X., Wei, Y., Tong, W., Tower, R.J., Chandra, A., Wang, L., Sun, Z., Yang, Z., Badar, F., Zhang, K., Tseng, W.J., Kramer, I., Kneissel, M., Xia, Y., Liu, X.S., Wang, J. H.C., Han, L., Enomoto-Iwamoto, M., Qin, L., 2018. Loading-induced reduction in sclerostin as a mechanism of subchondral bone plate sclerosis in mouse knee joints during late-stage osteoarthritis. Arthritis Rheumatol. 70 (2), 230–241.
Kaya, S., Basta-Pljakic, J., Seref-Ferlengez, Z., Majeska, R.J., Cardoso, L., Bromage, T.G., Zhang, Q., Flach, C.R., Mendelsohn, R., Yakar, S., Fritton, S.P., Schaffler, M.B., 2017. Lactation-induced changes in the volume of osteocyte lacunar-canalicular space Alter mechanical properties in cortical bone tissue. J. Bone Miner. Res. 32 (4), 688–697.
Kaya, S., Schurman, C.A., Dole, N.S., Evans, D.S., Alliston, T., 2022. Prioritization of genes relevant to bone fragility through the unbiased integration of aging mouse bone transcriptomics and human GWAS analyses. J. Bone Miner. Res. 37 (4), 804–817.
Kelly, N.H., Schimenti, J.C., Patrick Ross, F., van der Meulen, M.C., 2014. A method for isolating high quality RNA from mouse cortical and cancellous bone. Bone 68, 1–5.
Lindner, C., Thiagarajah, S., Wilkinson, J.M., Panoutsopoulou, K., Day-Williams, A.G., Arc, O.C., Cootes, T.F., Wallis, G.A., 2015. Investigation of association between hip osteoarthritis susceptibility loci and radiographic proximal femur shape. Arthritis Rheumatol. 67 (8), 2076–2084.
Love, M.I., Huber, W., Anders, S., 2014. Moderated estimation of fold change and dispersion for RNA-seq data with DESeq2. Genome Biol. 15 (12), 550.
Lynch, J.A., Parimi, N., Chaganti, R.K., Nevitt, M.C., Lane, N.E., G. Study of Osteoporotic Fractures Research, 2009. The association of proximal femoral shape and incident radiographic hip OA in elderly women. Osteoarthr. Cartil. 17 (10), 1313–1318.
Mazur, C.M., Woo, J.J., Yee, C.S., Fields, A.J., Acevedo, C., Bailey, K.N., Kaya, S., Fowler, T.W., Lotz, J.C., Dang, A., Kuo, A.C., Vail, T.P., Alliston, T., 2019. Osteocyte dysfunction promotes osteoarthritis through MMP13-dependent suppression of subchondral bone homeostasis. Bone Res. 7, 34.
McIntosh, I., Dreyer, S.D., Clough, M.V., Dunston, J.A., Eyaid, W., Roig, C.M., Montgomery, T., Ala-Mello, S., Kaitila, I., Winterpacht, A., Zabel, B., Frydman, M., Cole, W.G., Francomano, C.A., Lee, B., 1998. Mutation analysis of LMX1B gene in nail-patella syndrome patients. Am. J. Hum. Genet. 63 (6), 1651–1658.
Meakin, L.B., Galea, G.L., Sugiyama, T., Lanyon, L.E., Price, J.S., 2014. Age-related impairment of bones' adaptive response to loading in mice is associated with sex-related deficiencies in osteoblasts but no change in osteocytes. J. Bone Miner. Res. 29 (8), 1859–1871.
Morales Martinez, A., Caliva, F., Flament, I., Liu, F., Lee, J., Cao, P., Shah, R., Majumdar, S., Pedoia, V., 2020. Learning osteoarthritis imaging biomarkers from bone surface spherical encoding. Magn. Reson. Med. 84 (4), 2190–2203.
Morris, J.A., Kemp, J.P., Youlten, S.E., Laurent, L., Logan, J.G., Chai, R.C., Vulpescu, N. A., Forgetta, V., Kleinman, A., Mohanty, S.T., Sergio, C.M., Quinn, J., Nguyen-Yamamoto, L., Luco, A.L., Vijay, J., Simon, M.M., Pramatarova, A., Medina-Gomez, C., Trajanoska, K., Ghirardello, E.J., Butterfield, N.C., Curry, K.F., Leitch, V. D., Sparkes, P.C., Adoum, A.T., Mannan, N.S., Komla-Ebri, D.S.K., Pollard, A.S., Dewhurst, H.F., Hassall, T.A.D., Beltejar, M.G., , T. andMe Research, Adams, D.J., Vaillancourt, S.M., Kaptoge, S., Baldock, P., Cooper, C., Reeve, J., Ntzani, E.E., Evangelou, E., Ohlsson, C., Karasik, D., Rivadeneira, F., Kiel, D.P., Tobias, J.H., Gregson, C.L., Harvey, N.C., Grundberg, E., Goltzman, D., Adams, D.J., Lelliott, C.J., Hinds, D.A., Ackert-Bicknell, C.L., Hsu, Y.H., Maurano, M.T., Croucher, P.I., Williams, G.R., Bassett, J.H.D., Evans, D.M., Richards, J.B., 2019. An atlas of genetic influences on osteoporosis in humans and mice. Nat. Genet. 51 (2), 258–266.
Murray, C.J., Vos, T., Lozano, R., Naghavi, M., Flaxman, A.D., Michaud, C., Ezzati, M., Shibuya, K., Salomon, J.A., Abdalla, S., Aboyans, V., Abraham, J., Ackerman, I., Aggarwal, R., Ahn, S.Y., Ali, M.K., Alvarado, M., Anderson, H.R., Anderson, L.M., Andrews, K.G., Atkinson, C., Baddour, L.M., Bahalim, A.N., Barker-Collo, S., Barrero, L.H., Bartels, D.H., Basanez, M.G., Baxter, A., Bell, M.L., Benjamin, E.J., Bennett, D., Bernabe, E., Bhalla, K., Bhandari, B., Bikbov, B., Abdulhak, A.Bin, Birbeck, G., Black, J.A., Blencowe, H., Blore, J.D., Blyth, F., Bolliger, I., Bonaventure, A., Boufous, S., Bourne, R., Boussinesq, M., Braithwaite, T., Brayne, C., Bridgett, L., Brooker, S., Brooks, P., Brugha, T.S., Bryan-Hancock, C., Bucello, C., Buchbinder, R., Buckle, G., Budke, C.M., Burch, M., Burney, P., Burstein, R., Calabria, B., Campbell, B., Canter, C.E., Carabin, H., Carapetis, J., Carmona, L., Cella, C., Charlson, F., Chen, H., Cheng, A.T., Chou, D., Chugh, S.S., Coffeng, L.E., Colan, S.D., Colquhoun, S., Colson, K.E., Condon, J., Connor, M.D., Cooper, L.T., Corriere, M., Cortinovis, M., de Vaccaro, K.C., Couser, W., Cowie, B.C., Criqui, M.H., Cross, M., Dabhadkar, K.C., Dahiya, M., Dahodwala, N., Damsere-Derry, J., Danaei, G., Davis, A., Leo, D.De, Degenhardt, L., Dellavalle, R., Delossantos, A., Denenberg, J., Derrett, S., Jarlais, D.C.Des, Dharmaratne, S.D., Dherani, M., Diaz-Torne, C., Dolk, H., Dorsey, E.R., Driscoll, T., Duber, H., Ebel, B., Edmond, K., Elbaz, A., Ali, S.E., Erskine, H., Erwin, P.J., Espindola, P., Ewoigbokhan, S.E., Farzadfar, F., Feigin, V., Felson, D.T., Ferrari, A., Ferri, C.P., Fevre, E.M., Finucane, M.M., Flaxman, S., Flood, L., Foreman, K., Forouzanfar, M.H., Fowkes, F. G., Fransen, M., Freeman, M.K., Gabbe, B.J., Gabriel, S.E., Gakidou, E., Ganatra, H. A., Garcia, B., Gaspari, F., Gillum, R.F., Gmel, G., Gonzalez-Medina, D., Gosselin, R., Grainger, R., Grant, B., Groeger, J., Guillemin, F., Gunnell, D., Gupta, R., Haagsma, J., Hagan, H., Halasa, Y.A., Hall, W., Haring, D., Haro, J.M., Harrison, J.E., Havmoeller, R., Hay, R.J., Higashi, H., Hill, C., Hoen, B., Hoffman, H., Hotez, P.J., Hoy, D., Huang, J.J., Ibeanusi, S.E., Jacobsen, K.H., James, S.L., Jarvis, D., Jasrasaria, R., Jayaraman, S., Johns, N., Jonas, J.B., Karthikeyan, G., Kassebaum, N., Kawakami, N., Keren, A., Khoo, J.P., King, C.H., Knowlton, L.M., Kobusingye, O., Koranteng, A., Krishnamurthi, R., Laden, F., Lalloo, R., Laslett, L.L., Lathlean, T., Leasher, J.L., Lee, Y.Y., Leigh, J., Levinson, D., Lim, S.S., Limb, E., Lin, J.K., Lipnick, M., Lipshultz, S.E., Liu, W., Loane, M., Ohno, S.L., Lyons, R., Mabweijano, J., MacIntyre, M.F., Malekzadeh, R., Mallinger, L., Manivannan, S., Marcenes, W., March, L., Margolis, D.J., Marks, G.B., Marks, R., Matsumori, A., Matzopoulos, R., Mayosi, B.M., McAnulty, J.H., McDermott, M.M., McGill, N., McGrath, J., Medina-Mora, M.E., Meltzer, M., Mensah, G.A., Merriman, T.R., Meyer, A.C., Miglioli, V., Miller, M., Miller, T.R., Mitchell, P.B., Mock, C., Mocumbi, A.O., Moffitt, T.E., Mokdad, A.A., Monasta, L., Montico, M., Moradi-Lakeh, M., Moran, A., Morawska, L., Mori, R., Murdoch, M.E., Mwaniki, M.K., Naidoo, K., Nair, M.N., Naldi, L., Narayan, K.M., Nelson, P.K., Nelson, R.G., Nevitt, M.C., Newton, C.R., Nolte, S., Norman, P., Norman, R., O'Donnell, M., O'Hanlon, S., Olives, C., Omer, S.B., Ortblad, K., Osborne, R., Ozgediz, D., Page, A., Pahari, B., Pandian, J.D., Rivero, A.P., Patten, S.B., Pearce, N., Padilla, R.P., Perez-Ruiz, F., Perico, N., Pesudovs, K., Phillips, D., Phillips, M.R., Pierce, K., Pion, S., Polanczyk, G.V., Polinder, S., Pope III, C.A., Popova, S., Porrini, E., Pourmalek, F., Prince, M., Pullan, R.L., Ramaiah, K.D., Ranganathan, D., Razavi, H., Regan, M., Rehm, J.T., Rein, D.B., Remuzzi, G., Richardson, K., Rivara, F.P., Roberts, T., Robinson, C., Leon, F.R.De, Ronfani, L., Room, R., Rosenfeld, L.C., Rushton, L., Sacco, R.L., Saha, S., Sampson, U., Sanchez-Riera, L., Sanman, E., Schwebel, D.C., Scott, J.G., Segui-Gomez, M., Shahraz, S., Shepard, D.S., Shin, H., Shivakoti, R., Singh, D., Singh, G.M., Singh, J.A., Singleton, J., Sleet, D.A., Sliwa, K., Smith, E., Smith, J.L., Stapelberg, N.J., Steer, A., Steiner, T., Stolk, W.A., Stovner, L.J., Sudfeld, C., Syed, S., Tamburlini, G., Tavakkoli, M., Taylor, H.R., Taylor, J.A., Taylor, W.J., Thomas, B., Thomson, W.M., Thurston, G.D., Tleyjeh, I.M., Tonelli, M., Towbin, J.A., Truelsen, T., Tsilimbaris, M.K., Ubeda, C., Undurraga, E.A., van der Werf, M.J., van Os, J., Vavilala, M.S., Venketasubramanian, N., Wang, M., Wang, W., Watt, K., Weatherall, D.J., Weinstock, M.A., Weintraub, R., Weisskopf, M.G., Weissman, M.M., White, R.A., Whiteford, H., Wiebe, N., Wiersma, S.T., Wilkinson, J. D., Williams, H.C., Williams, S.R., Witt, E., Wolfe, F., Woolf, A.D., Wulf, S., Yeh, P.H., Zaidi, A.K., Zheng, Z.J., Zonies, D., Lopez, A.D., AlMazroa, M.A., Memish, Z.A., 2012. Disability-adjusted life years (DALYs) for 291 diseases and injuries in 21 regions, 1990-2010: a systematic analysis for the Global Burden of Disease Study 2010. Lancet 380 (9859), 2197–2223.
Nakasa, T., Adachi, N., Kato, T., Ochi, M., 2014. Correlation between subchondral bone plate thickness and cartilage degeneration in osteoarthritis of the ankle. Foot Ankle Int. 35 (12), 1341–1349.
Neogi, T., Bowes, M.A., Niu, J., De Souza, K.M., Vincent, G.R., Goggins, J., Zhang, Y., Felson, D.T., 2013. Magnetic resonance imaging-based three-dimensional bone shape of the knee predicts onset of knee osteoarthritis: data from the osteoarthritis initiative. Arthritis Rheum. 65 (8), 2048–2058.
Nielsen, A.W., Klose-Jensen, R., Hartlev, L.B., Boel, L.W.T., Thomsen, J.S., Keller, K.K., Hauge, E.M., 2019. Age-related histological changes in calcified cartilage and subchondral bone in femoral heads from healthy humans. Bone 129, 115037.
Niimori, D., Kawano, R., Felemban, A., Niimori-Kita, K., Tanaka, H., Ihn, H., Ohta, K., 2012. Tsukushi controls the hair cycle by regulating TGF-beta1 signaling. Dev. Biol. 372 (1), 81–87.
Okura, T., Matsushita, M., Mishima, K., Esaki, R., Seki, T., Ishiguro, N., Kitoh, H., 2018. Activated FGFR3 prevents subchondral bone sclerosis during the development of osteoarthritis in transgenic mice with achondroplasia. J. Orthop. Res. 36 (1), 300–308.
Pantano, L., 2022. DEGreport: report of DEG analysis. Github. http://lpantano.github.io/DEGreport.
Ries, C., Boese, C.K., Sturznickel, J., Koehne, T., Hubert, J., Pastor, M.F., Hahn, M., Meier, S.L., Beil, F.T., Puschel, K., Amling, M., Rolvien, T., 2020. Age-related changes of micro-morphological subchondral bone properties in the healthy femoral head. Osteoarthr. Cartil. 28 (11), 1437–1447.
Rodriguez, R.R., Seegmiller, R.E., Stark, M.R., Bridgewater, L.C., 2004. A type XI collagen mutation leads to increased degradation of type II collagen in articular cartilage. Osteoarthr. Cartil. 12 (4), 314–320.

Sacitharan, P.K., Vincent, T.L., 2016. Cellular ageing mechanisms in osteoarthritis. Mamm. Genome 27 (7–8), 421–429.
Schurman, C.A., Verbruggen, S.W., Alliston, T., 2021. Disrupted osteocyte connectivity and pericellular fluid flow in bone with aging and defective TGF-beta signaling. Proc. Natl. Acad. Sci. U. S. A. 118 (25).
Shao, Y., Zhao, C., Pan, J., Zeng, C., Zhang, H., Liu, L., Fan, K., Liu, X., Luo, B., Fang, H., Bai, X., Zhang, H., Cai, D., 2021. BMP5 silencing inhibits chondrocyte senescence and apoptosis as well as osteoarthritis progression in mice. Aging (Albany NY) 13 (7), 9646–9664.
Shepherd, C., Zhu, D., Skelton, A.J., Combe, J., Threadgold, H., Zhu, L., Vincent, T.L., Stuart, P., Reynard, L.N., Loughlin, J., 2018. Functional characterization of the osteoarthritis genetic risk residing at ALDH1A2 identifies rs12915901 as a key target variant. Arthritis Rheumatol. 70 (10), 1577–1587.
Styrkarsdottir, U., Lund, S.H., Thorleifsson, G., Zink, F., Stefansson, O.A., Sigurdsson, J. K., Juliusson, K., Bjarnadottir, K., Sigurbjornsdottir, S., Jonsson, S., Norland, K., Stefansdottir, L., Sigurdsson, A., Sveinbjornsson, G., Oddsson, A., Bjornsdottir, G., Gudmundsson, R.L., Halldorsson, G.H., Rafnar, T., Jonsdottir, I., Steingrimsson, E., Norddahl, G.L., Masson, G., Sulem, P., Jonsson, H., Ingvarsson, T., Gudbjartsson, D. F., Thorsteinsdottir, U., Stefansson, K., 2018. Meta-analysis of icelandic and UK data sets identifies missense variants in SMO, IL11, COL11A1 and 13 more new loci associated with osteoarthritis. Nat. Genet. 50 (12), 1681–1687.
Styrkarsdottir, U., Thorleifsson, G., Helgadottir, H.T., Bomer, N., Metrustry, S., Bierma-Zeinstra, S., Strijbosch, A.M., Evangelou, E., Hart, D., Beekman, M., Jonasdottir, A., Sigurdsson, A., Eiriksson, F.F., Thorsteinsdottir, M., Frigge, M.L., Kong, A., Gudjonsson, S.A., Magnusson, O.T., Masson, G., , T.-O. Consortium, Arc, O.C., Hofman, A., Arden, N.K., Ingvarsson, T., Lohmander, S., Kloppenburg, M., Rivadeneira, F., Nelissen, R.G., Spector, T., Uitterlinden, A., Slagboom, P.E., Thorsteinsdottir, U., Jonsdottir, I., Valdes, A.M., Meulenbelt, I., van Meurs, J., Jonsson, H., Stefansson, K., 2014. Severe osteoarthritis of the hand associates with common variants within the ALDH1A2 gene and with rare variants at 1p31. Nat. Genet. 46 (5), 498–502.
Tachmazidou, I., Hatzikotoulas, K., Southam, L., Esparza-Gordillo, J., Haberland, V., Zheng, J., Johnson, T., Koprulu, M., Zengini, E., Steinberg, J., Wilkinson, J.M., Bhatnagar, S., Hoffman, J.D., Buchan, N., Suveges, D., Arc, O.C., Yerges-Armstrong, L., Smith, G.D., Gaunt, T.R., Scott, R.A., McCarthy, L.C., Zeggini, E., 2019. Identification of new therapeutic targets for osteoarthritis through genome-wide analyses of UK Biobank data. Nat. Genet. 51 (2), 230–236.
Tang, S.Y., Herber, R.P., Ho, S.P., Alliston, T., 2012. Matrix metalloproteinase-13 is required for osteocytic perilacunar remodeling and maintains bone fracture resistance. J. Bone Miner. Res. 27 (9), 1936–1950.
Therneau, T., Hart, S., Kocher, J.P., 2021. Calculating SamplesSize Estimates for RNA Seq Studies.
Tschon, M., Contartese, D., Pagani, S., Borsari, V., Fini, M., 2021. Gender and sex are key determinants in osteoarthritis not only confounding variables. A systematic review of clinical data. J. Clin. Med. 10 (14).
Van Wesenbeeck, L., Odgren, P.R., Coxon, F.P., Frattini, A., Moens, P., Perdu, B., MacKay, C.A., Van Hul, E., Timmermans, J.P., Vanhoenacker, F., Jacobs, R., Peruzzi, B., Teti, A., Helfrich, M.H., Rogers, M.J., Villa, A., Van Hul, W., 2007. Involvement of PLEKHM1 in osteoclastic vesicular transport and osteopetrosis in incisors absent rats and humans. J. Clin. Invest. 117 (4), 919–930.
Wilhelmi, G., Faust, R., 1976. Suitability of the C 57 black mouse as an experimental animal for the study of skeletal changes due to ageing, with special reference to osteo-arthrosis and its response to tribenoside. Pharmacology 14 (4), 289–296.
Wu, T., Hu, E., Xu, S., Chen, M., Guo, P., Dai, Z., Feng, T., Zhou, L., Tang, W., Zhan, L., Fu, X., Liu, S., Bo, X., Yu, G., 2021. clusterProfiler 4.0: a universal enrichment tool for interpreting omics data. Innovation (Camb) 2 (3), 100141.
Youlten, S.E., Kemp, J.P., Logan, J.G., Ghirardello, E.J., Sergio, C.M., Dack, M.R.G., Guilfoyle, S.E., Leitch, V.D., Butterfield, N.C., Komla-Ebri, D., Chai, R.C., Corr, A.P., Smith, J.T., Mohanty, S.T., Morris, J.A., McDonald, M.M., Quinn, J.M.W., McGlade, A.R., Bartonicek, N., Jansson, M., Hatzikotoulas, K., Irving, M.D., Beleza-Meireles, A., Rivadeneira, F., Duncan, E., Richards, J.B., Adams, D.J., Lelliott, C.J., Brink, R., Phan, T.G., Eisman, J.A., Evans, D.M., Zeggini, E., Baldock, P.A., Bassett, J. H.D., Williams, G.R., Croucher, P.I., 2021. Osteocyte transcriptome mapping identifies a molecular landscape controlling skeletal homeostasis and susceptibility to skeletal disease. Nat. Commun. 12 (1), 2444.
Yuan, R., Tsaih, S.W., Petkova, S.B., Marin de Evsikova, C., Xing, S., Marion, M.A., Bogue, M.A., Mills, K.D., Peters, L.L., Bult, C.J., Rosen, C.J., Sundberg, J.P., Harrison, D.E., Churchill, G.A., Paigen, B., 2009. Aging in inbred strains of mice: study design and interim report on median lifespans and circulating IGF1 levels. Aging Cell 8 (3), 277–287.